Ultrasound in Med. & Biol., Vol. 47, No. 4, pp. 1077–1088, 2021

0301-5629/$ - see front matter

https://doi.org/10.1016/j.ultrasmedbio.2020.12.011

● *Original Contribution*

MULTIFREQUENCY PHASED TRACKING METHOD FOR ESTIMATING VELOCITY IN HEART WALL

YU OBARA,* SHOHEI MORI,† MOTOTAKA ARAKAWA,*,† and HIROSHI KANAI*,†

* Graduate School of Biomedical Engineering, Tohoku University, Sendai, Japan; and † Graduate School of Engineering, Tohoku University, Sendai, Japan

(*Received* 17 *June* 2020; *revised* 1 *December* 2020; *in final from* 12 *December* 2020)

Abstract—Local high-accuracy velocity estimation is important for the ultrasound-based evaluation of regional myocardial function. The ultrasound phase difference at the center frequency of the transmitted signal has been conventionally used for velocity estimation. In the conventional method, spatial averaging is necessary owing to the frequency-dependent attenuation and interference of backscattered waves. Here, we propose a method for suppressing these effects using multifrequency phase differences. The resulting improvement in velocity estimation in the heart wall was validated by *in vivo* experiments. In the conventional method, the velocity waveform exhibits spike-like changes. The velocity waveform estimated using the proposed method did not exhibit such changes. Because the proposed method estimates myocardium velocity without spatial averaging, it can be used for measuring heart wall dynamics involving thickness changes. (E-mail: mori@ecei.tohoku.ac.jp)

Key Words: **Ultrasound, Heart wall, Measurement of displacement, Phase difference, Interference, Thickness change, Strain rate.**

INTRODUCTION

Ischemic heart diseases, such as myocardial infarction and cardiac angina, are the leading factors determining the number of years of life lost in 2016 (Foreman et al. 2018). Ischemic heart diseases negatively affect regional myocardial function. Therefore, there is a need to develop highly accurate and repeatable methods for evaluation of regional myocardial function; these diagnostic methods can help to prevent the onset of ischemic heart diseases and can increase the efficiency of post-onset treatment. Ultrasound-based diagnostic apparatuses are less expensive than other diagnostic apparatuses, such as computed tomography and/or magnetic resonance imaging apparatuses, and can be used for non-invasive real-time observation of organ dynamics. Given this, ultrasound-based medical evaluation methods have been popular.

Conventionally, B-mode and M-mode imaging have been used for evaluating myocardial contractile function (Mason et al. 1979; Shapiro et al. 1981; Guth et al. 1984). However, there are qualitative diagnosis methods that may be examiner dependent (Picano et al. 1991). Thus, it is necessary to develop quantitative diagnosis methods based on the physiologic mechanisms of myocardial contraction.

Many physiologic studies of myocardial contraction have confirmed that the myocardium contracts owing to electrical excitation (Durrer et al. 1970; McVeigh et al. 2002; Faris et al. 2003; Ramanathan et al. 2004; Pernot et al. 2007; Konofagou and Provost 2012; Grondin et al. 2019). Therefore, the minute contraction response accompanied by the conduction of electrical excitation has been measured in the time phase around the R-wave in the electrocardiogram, for regional myocardial function evaluation (Kanai and Tanaka 2011). When the myocardium contracts, its thickness increases owing to the volume conservation constraint. In previous studies in animal models using invasive methods, the regional myocardial function was evaluated quantitatively by measuring changes in myocardium thickness (Theroux et al. 1974; Heyndrickx et al. 1975; Sasayama et al. 1976; Sabbah et al. 1981; Hartley et al. 1983, 1991; Homans et al. 1985). Therefore, it is possible to measure

Address correspondence to: Shohei Mori, Graduate School of Engineering, Tohoku University, Sendai 980-8579, Japan. E-mail: mori@ecei.tohoku.ac.jp

myocardial contraction by observing changes in myocardium thickness. Measurements of local changes in myocardium thickness (Kanai et al. 2006), myocardial strain (Sutherland et al. 2004; Marwick 2006; Grondin et al. 2015) and myocardial strain rate (Kanai et al. 1997; Sutherland et al. 2004; Marwick 2006; Yoshiara et al. 2007; Tanaka et al. 2014a, 2014b, 2017, 2019) have been utilized for quantitative evaluation of myocardial contractile function. Moreover, the strain rate of the myocardium after the onset of ischemic heart diseases has been studied, and the difference between normal and infracted myocardia has been discussed (Jamal et al. 2002; Pislaru et al. 2004).

The changes in myocardium thickness, myocardial strain and myocardial strain rate are calculated from velocities at multiple positions in the myocardium. In addition to measuring the myocardium contraction based on changes in myocardium thickness, the minute contraction propagation velocity has been calculated from the delay times of myocardial velocity waveforms (Matsuno et al. 2017; Hayashi et al. 2019). Therefore, it is important to estimate myocardial local velocity with high accuracy.

We have estimated the velocity in the ultrasound beam direction using the phased-tracking method (Kanai et al. 1996; Kanai et al. 1997). In the conventional method, the quadrature detection method was applied to the received signal at the center frequency of the transmitted signal (Kanai et al. 1996, 1997, 2006; Yoshiara et al. 2007; Tanaka et al. 2014a, 2014b, 2017; Matsuno et al. 2017; Hayashi et al. 2019), and the velocity was estimated using the phase difference between the received signals at the center frequency of the transmitted signal. However, the peak frequency of the received signal does not correspond to the center frequency of the transmitted signal, as it depends on two factors. One of these factors is the attenuation that occurs when the ultrasound wave propagates through living tissue. Owing to the frequency dependence of this attenuation, the signal's high-frequency components are attenuated more than its low-frequency components especially for signals reflected from deep-tissue regions. Therefore, the peak frequency of the received signal is lower than the center frequency of the transmitted signal. The other important factor is the interference of backscattered waves from numerous scatterers in the myocardium. Because this interference depends on the scatterers' spacing, the signal-to-noise ratio (SNR) may decrease at a certain frequency of the received signal affected by the destructive interference. Thus, the peak frequency of the received signal can be interference dependent (Hasegawa and Kanai 2008a). Therefore, the conventional method is sensitive with respect to destructive interference, which decreases the SNR at the center frequency of the transmitted signal.

Here, we propose a method for local and highly accurate estimation of myocardial velocity waveforms using the phased-tracking method extended to multiple frequencies. By calculating such multifrequency phase differences, even when the SNR at a certain frequency is low, the phase differences at other frequencies (with high SNRs) can be used to estimate velocity waveforms. A velocity estimator that uses multifrequency phase differences has been considered in several previous studies. One of them is the phase-sensitive 2-D motion estimator proposed by Hasegawa (2016). The primary objective of that study was to expand a 2-D motion estimator using the phase at a specific frequency (Salles et al. 2015) to one that uses multifrequency phases, to improve the estimation accuracy of the displacement in the lateral direction, that is, perpendicular to the beam axis, using a smaller spatial window. However, the effects of attenuation and interference of scattered waves have not been studied thoroughly. In the present study, the main purpose of the proposed method is to suppress the influence of the attenuation and interference of scattered waves in the heart wall dynamics measurements, where myocardium thickness changes owing to myocardium contraction.

We compared the proposed phased-tracking method extended to multiple frequencies with the conventional phased-tracking method that uses the phase difference at the center frequency of the transmitted signal, and evaluated the reproducibility of the velocity waveforms estimated using the proposed method. We discuss the usefulness of the proposed method for measuring heart wall dynamics involving thickness changes.

METHODS

Conventional method

The conventional phased-tracking method (Kanai et al. 1996, 1997) at the center frequency of the transmitted signal is explained below and in Figure 1. (I)

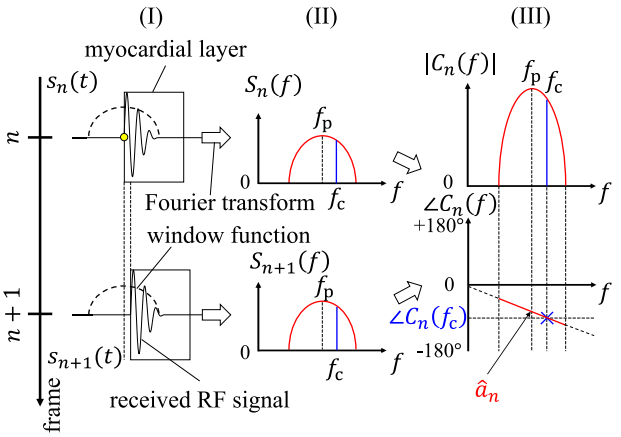

Fig. 1. Schematic of the estimation of velocity using the phase gradient of the cross-spectrum in the conventional method (*blue lines*) and in the proposed method (*red lines*). RF = radiofrequency.

The received radiofrequency (RF) signal $s_n(t)$ around the analysis point in the nth frame is cut out using a window function. (II) The complex frequency spectrum $S_n(f)$ is obtained using the discrete Fourier transform (DFT). The DFT is also applied to the received signal $s_{n+1}(t)$ of the $(n+1)$th frame. (III) The cross-spectrum $C_n(f)$ between the consecutive frames is calculated as

$$C_n(f) = S_n^*(f) \cdot S_{n+1}(f) \tag{1}$$

where $*$ denotes the complex conjugate. The amplitude of the cross-spectrum, $|C_n(f)|$, represents the correlation, in the frequency domain, between the frames of the received signal, and the phase $\angle C_n(f)$ of the cross-spectrum represents the phase difference between the frames of the received signal. The estimated velocity $\hat{v}_d(n)$ is calculated as

$$\hat{v}_d(n) = \frac{c_0 f_{FR}}{4\pi} \cdot \frac{-\angle C_n(f_c)}{f_c} \tag{2}$$

where c_0 is the speed of sound in the living tissue, f_{FR} is the frame rate and f_c is the center frequency of the transmitted signal.

Proposed method

The proposed phased-tracking method, which is extended to multiple frequencies, is described below. Assuming that the velocity $v_d(n)$ between the frames is uniform in the window of the DFT and the phase $\angle C_n(f)$ of the cross-spectrum is linear, the phase gradient a_n of the cross-spectrum is expressed as

$$a_n = -\frac{4\pi}{c_0 f_{FR}} \cdot v_d(n) \tag{3}$$

Therefore, the velocity $v_d(n)$ between the consecutive frames can be calculated from the phase gradient a_n of the cross-spectrum.

In the proposed method, the phase gradient a_n of the cross-spectrum is estimated from the phase $\angle C_n(f)$ with multiple frequencies. Assuming that the cross-spectrum phase is linear, the root mean squared error (RMSE) of the estimated phase gradient, $\alpha_n(a)$, weighted by the cross-spectrum amplitude $|C_n(f)|$, is defined as

$$\alpha_n(a) = \sqrt{\frac{\sum_{f=0}^{\frac{f_s}{2}} |C_n(f)| \cdot |\angle C_n(f) - af|^2}{\sum_{f=0}^{\frac{f_s}{2}} |C_n(f)|}} \tag{4}$$

for the sampling frequency f_s and arbitrary variable a. When the value of af is greater than (less than) 180°, 360° is subtracted (added) from (to) the value of af to deal with aliasing. From eqn (3), the velocity $\hat{v}_d(n)$ can be estimated from the phase gradient $\hat{a}_n$ of the cross-spectrum that minimizes the RMSE $\alpha_n(a)$. The velocity is calculated as

$$\hat{v}_d(n) = \frac{c_0 f_{FR}}{4\pi} \cdot (-\hat{a}_n) \tag{5}$$

$$\hat{a}_n = \arg\min_a \alpha_n(a) \tag{6}$$

The concept underlying this estimation method is the same as that underlying the phase-sensitive 2-D motion estimator proposed by Hasegawa (2016); however, the main purpose is different, as mentioned in the Introduction.

Figure 1 schematically illustrates estimation of the velocity using the phase gradient of the cross-spectrum in the conventional and proposed methods. The *blue lines* represent the spectra and phases for the conventional method, whereas the *red lines* represent the spectra and phases for the proposed method. In the conventional method, the estimation accuracy of the cross-spectrum phase might be lower, owing to the influence of attenuation and the interference, because only the phase at the center frequency of the transmitted signal is used. Because the higher-frequency components of the ultrasound wave are more attenuated, the peak frequency f_p of the signal received from the heart wall is lower than the center frequency f_c of the transmitted signal, as illustrated in Figure 1. Therefore, in the conventional method, the velocity might be estimated from the phase difference at the frequency with a low SNR of the cross-spectrum.

Furthermore, the phase difference at a certain frequency may be affected by the interference, depending on the position of the myocardium to be analyzed. Because there are numerous scatterers in the myocardium that are smaller than the resolution of the ultrasound wave, the received signal is the interference of numerous backscattered waves. When destructive interference occurs, for example, as a result of the opposite phase in assuming two scatterers, the SNR decreases dramatically, and the cross-spectrum phase cannot be calculated accurately. When destructive interference occurs at the center frequency of the transmitted signal, the estimation accuracy of the velocity using the conventional method with the phase difference at the center frequency of the transmitted signal becomes lower. In the proposed method, the cross-spectrum phase gradient $\hat{a}_n$ is estimated by using the cross-spectrum amplitude $|C_n(f)|$ as the weighting function. Therefore, the influence of the phase difference at the frequency at which the SNR is lower owing to the attenuation and/or interference can be suppressed.

Measurement environment

In vivo measurements were made on the interventricular septum (IVS) of healthy subjects in their early twenties, using ultrasound diagnostic apparatuses. The measurement was approved by the Ethics Committee of Tohoku University, and the subjects agreed to participate in this study. For measurement of subjects A, B and C, a plane wave with the

center frequency f_c of 3.75 MHz was transmitted from a sector probe (UST-52101 N; Hitachi-Aloka-Medical Ltd, Tokyo, Japan) connected to an ultrasonic diagnostic apparatus (Prosound α-10; Hitachi-Aloka-Medical Ltd, Tokyo, Japan), and high-frame-rate measurements (f_{FR} = 860 Hz) were made using parallel beamforming (Hasegawa and Kanai 2008b). The sampling frequency f_s was 15 MHz, and the sound velocity c_0 in the living tissue was assumed to be 1540 m/s; thus, the depth interval of the sampling points was 0.051 mm. For measurement of subjects D, E and F, a focused wave with the center frequency f_c of 3.75 MHz was transmitted from a sector probe (UST-52101; Hitachi-Aloka-Medical Ltd, Tokyo, Japan) connected to an ultrasonic diagnostic apparatus (SSD6500; Hitachi-Aloka-Medical Ltd, Tokyo, Japan). By reducing the number of beams, high-frame-rate measurement ($f_{FR} \geq$ 630 Hz) was realized. The sampling frequency f_s was 20 MHz, and the sound velocity c_0 in the living tissue was assumed to be 1540 m/s; thus, the depth interval of the sampling points was 0.038 mm.

In these measurements, the electrocardiogram (ECG) and phonocardiogram (PCG) were acquired simultaneously. For each subject, the ECG was measured using the three-point lead method, and the ECG waveform was obtained for lead II. The PCG waveform was measured using a small microphone attached to the subject's chest.

Figure 2 is the initial-frame B-mode image of a subject and the analysis point where the velocity was estimated (*yellow point*). Around the time phase of the ECG R-wave representing the onset of the minute contraction response, the velocity at the analysis point was estimated using the phased-tracking method at the center frequency of the transmitted signal (conventional method, eqn (2)) and using multiple frequencies (proposed method, eqn (5)). In the velocity estimation, the received RF signal

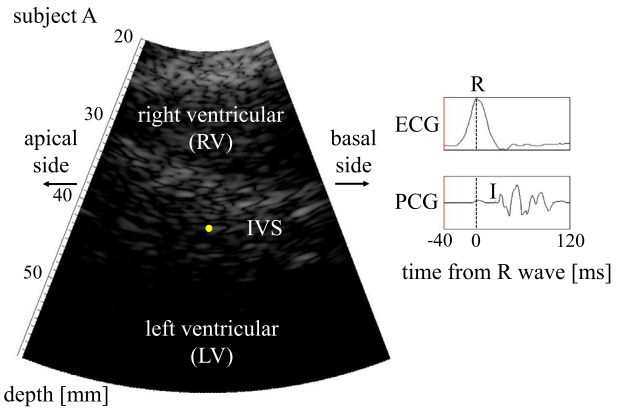

Fig. 2. B-mode image of the left ventricle in the long-axis view and the analyzed point at which the velocity was estimated (*yellow point*). ECG = electrocardiogram; PCG = phonocardiogram.

was cut out using the Hanning window in the range of ±1.22 mm around the analysis point in the depth direction. Then, the cross-spectrum $C_n(f)$ in eqn (1) was obtained, and the velocity between two consecutive frames was estimated. The analysis point was moved with the movement of IVS. The movement of IVS was measured by integrating the estimated velocity waveform.

To compare the proposed method with the conventional method using the RMSE $\alpha_n(a)$ in eqn (4), there was a need to calculate the RMSE in the conventional method. Therefore, the phase gradient of the cross-spectrum $\hat{a}_n$ in eqn (4) was taken place by $\angle C_n(f_c)/f_c$ to calculate the RMSE for the conventional method using the phase at the center frequency of the transmitted signal.

RESULTS

Figure 3 illustrates (a) the ECG waveform, (b) the PCG waveform, (c) the velocity waveform and (d) the RMSE in the phase gradient estimation. On the vertical axis in Figure 3c, a downward positive value indicates the contraction movement toward the left ventricle (LV), and an upward negative value indicates the movement toward the right ventricle (RV). The *dotted lines* represent the maximal velocities that can be measured using the phase difference at the center frequency f_c of the transmitted signal. The horizontal axis is the time from the ECG R-wave. Figure 3c, 3d illustrates the results obtained using the phased-tracking method extended to multiple frequencies (proposed method, *red lines*) and using the method that uses only the center frequency f_c of the transmitted signal (conventional method, *blue lines*).

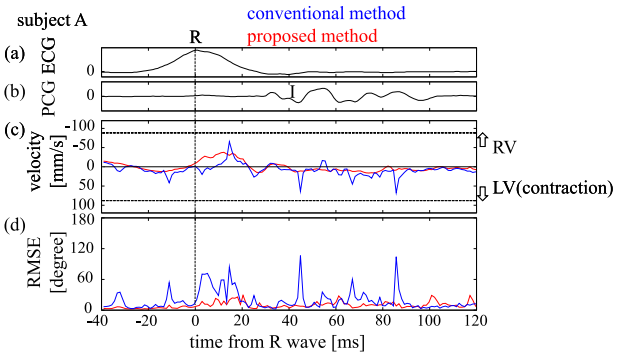

Fig. 3. (a) Electrocardiogram (ECG) waveform, (b) phonocardiogram (PCG) waveform, (c) velocity waveform and (d) minimal root mean square error (RMSE) of the phase gradient estimation, where *blue lines* represent the results obtained using the conventional method, which uses the phase difference at the center frequency of the transmitted signal, and *red lines* represent the results obtained using the proposed method that uses phase differences with multiple frequencies. LV = left ventricle; RV = right ventricle.

The velocity waveform estimated using the conventional method exhibited spike-like changes, while the waveform estimated using the proposed method did not exhibit spike-like changes. Moreover, when the velocity waveform estimated using the conventional method exhibited spike-like changes, the RMSE in the conventional method was extremely large compared with that in the proposed method. This suggests that the spike-like velocity changes observed for the estimation using the conventional method could be attributed to the erroneous estimation.

Let us discuss the cause of the spike-like velocity change in the velocity waveform estimated using the conventional method. We focused on the detail of the velocity estimation for the n_1th frame (44.9 ms from the ECG R-wave) with the maximal RMSE for the conventional method in Figure 3d, at which the positive spike-like velocity change was estimated as illustrated in Figure 3c. Figure 4 illustrates (a) the received RF signals before cutting out using the Hanning window, (b) the amplitudes of the complex frequency spectra, $|S_n(f)|$, (c) the phases of the complex frequency spectra, $\angle S_n(f)$, (d) the amplitude of the cross-spectrum, $|C_n(f)|$, and (e) the phase of the cross-spectrum, $\angle C_n(f)$. In Figure 4a–c, the *blue lines* correspond to the frequency spectrum $S_n(f)$ of the frame with the maximal RMSE, for the conventional method, while the *red lines* correspond to the frequency spectrum $S_{n+1}(f)$ in the next frame. In Figure 4d, 4e, the *solid lines* represent the cross-spectrum $C_n(f)$ between the nth and $(n+1)$th frames, the point (×) represents the cross-spectrum phase $\angle C_n(f_c)$ at the center frequency f_c of the transmitted signal, for the conventional method, and the *red dashed line* represents the gradient of the cross-spectrum phase $\hat{a}_n$ estimated using the proposed method with multiple frequencies.

In Figure 4b, the peak frequency of the received signal is lower than the center frequency f_c of the transmitted signal. This is attributed to the frequency-dependent attenuation. Despite the frequency-dependent attenuation, $|S_n(f_c)|$ and $|S_{n+1}(f_c)|$ are lower than the amplitude of the complex frequency spectrum at the adjacent frequency, which is approximately 4 MHz. This is attributed to the destructive interference. Although the analyzed position in the myocardium was the same, $|S_n(f)|$ differs from $|S_{n+1}(f)|$. This is attributed to the change in the interference state. In Figure 4d, the peak frequency f_p of the cross-spectrum amplitude $|C_n(f)|$ is approximately 3 MHz. The cross-spectrum amplitude at the center frequency f_c of the transmitted signal $|C_n(f_c)|$ is −37 dB in Figure 4d, relative to that at the peak frequency f_p of the received signal. In Figure 4e, the phase of the cross-spectrum, $\angle C_n(f_c)$, at the center frequency f_c of the transmitted signal is significantly different from the phase at the peak frequency. These results indicate that the SNR decreased at the center frequency f_c of the transmitted signal owing to the influence of the attenuation and the interference, and $\angle C_n(f_c)$ used in the conventional method was not calculated as the phase difference reflecting the actual heart wall motion. On the other hand, the attenuation and interference effects were suppressed in the proposed method, because the estimated cross-phase gradient $\hat{a}_n$ was calculated from the phase difference with multiple frequencies using the cross-spectrum amplitude $|C_n(f)|$ as a weighting function. In Figure 4d, the 20-dB bandwidth in the velocity estimation was 2.45−3.37 MHz.

We evaluated the reproducibility of the velocity waveforms estimated using the proposed method. Figures 5−7 illustrate the results around the time phase of

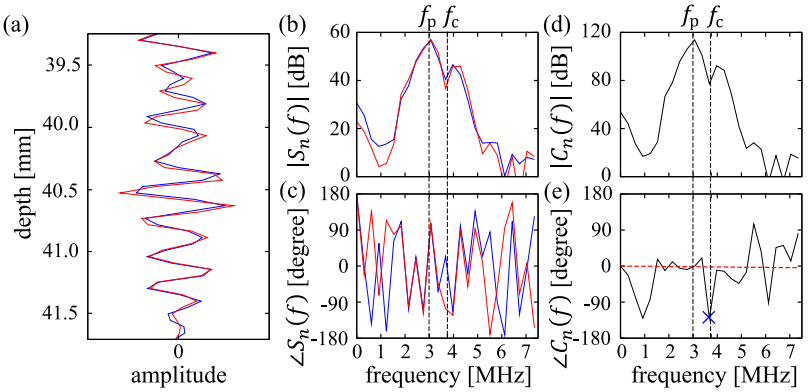

Fig. 4. (a) Received radiofrequency signal $s_{n_1}(t)$, (b) amplitude of the complex frequency spectrum, $|S_{n_1}(f)|$, and (c) phase of the complex frequency spectrum, $\angle S_{n_1}(f)$, where the *blue line* represents $S_{n_1}(f)$, where RMSE was maximal for the conventional method, and the *red line* represents $S_{n_1+1}(f)$. (d) The amplitude of the cross-spectrum, $|C_{n_1}(f)|$, of the n_1th frame with maximal root mean square error (RMSE) in the conventional method and (e) phase of the cross-spectrum, $\angle C_{n_1}(f)$, where the *dashed line* represents the phase gradient of the cross-spectrum, $\hat{a}_{n_1}$, estimated using the proposed method, and the symbol × indicates the cross-spectrum phase $\angle C_{n_1}(f_c)$ at the center frequency of the transmitted signal, using the conventional method. ECG = electrocardiogram; PCG = phonocardiogram.

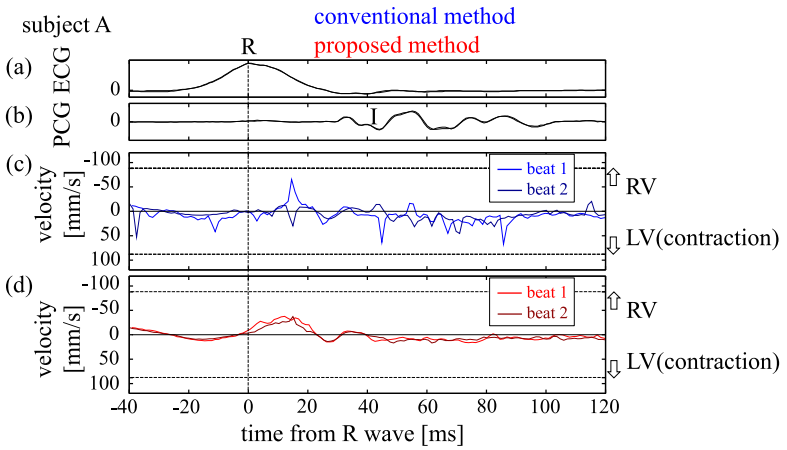

Fig. 5. Results of the estimated velocity waveform for subject A in two consecutive heartbeats. (a) Electrocardiogram (ECG) waveform. (b) Phonocardiogram (PCG) waveform. (c) Velocity waveform estimated using the conventional method that uses the phase difference at a single center frequency of the transmitted signal. (d) Velocity waveform estimated using the proposed method that uses phase differences with multiple frequencies. LV = left ventricle; RV = right ventricle.

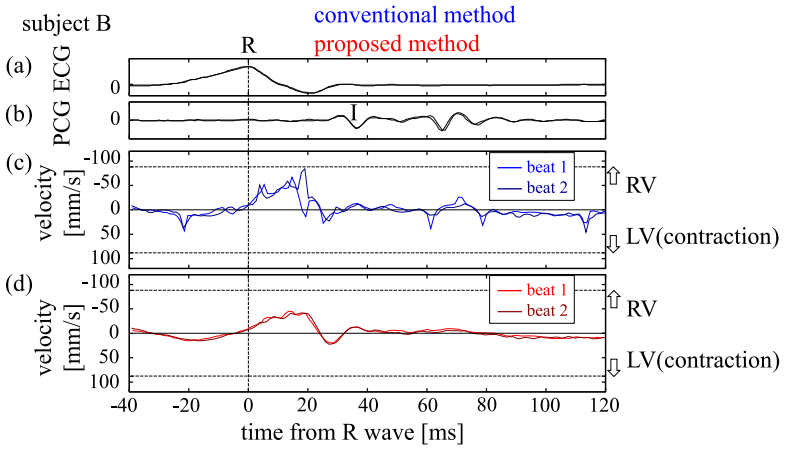

Fig. 6. Results of the estimated velocity waveform for subject B in two consecutive heartbeats. (a) Electrocardiogram (ECG) waveform. (b) Phonocardiogram (PCG) waveform. (c) Velocity waveform estimated using the conventional method that uses the phase difference at the center frequency of the transmitted signal. (d) Velocity waveform estimated using the proposed method that uses phase differences with multiple frequencies. LV = left ventricle; RV = right ventricle.

the ECG R-wave for two consecutive heartbeats and for different subjects. The velocity waveforms estimated using the proposed method are provided in Figures 5d, 6d and 7d and are quite similar. On the other hand, the velocity waveforms estimated using the conventional method are provided in Figures 5c, 6c and 7c and are quite different because spike-like velocity changes owing to the lower SNR occur independently from the heart wall dynamics. In Figure 7c, the velocity waveforms estimated using the conventional method exhibit steep discontinuity, which is caused by aliasing after 20 ms from the R-wave. This is because the velocity in the heart wall exceeded the maximal velocity that can be measured using the phase difference at the center frequency f_c of the transmitted signal. In the proposed method, the velocity was estimated using the phase gradient of the cross-spectrum. In the proposed method, if the change in the cross-spectrum phase between adjacent frequency components was less than 180°, the phase gradient of the cross-spectrum can be calculated without aliasing. In the present measurement, the change in the cross-spectrum phase between the peak frequency and its adjacent frequency was approximately 10°. Therefore, in the proposed method, the velocity was measured without aliasing. For measurement of subjects D, E and F, the reproducibility of the velocity waveforms was evaluated by calculating the standard deviation (SD) in four consecutive heartbeats. The values of the SD averaged

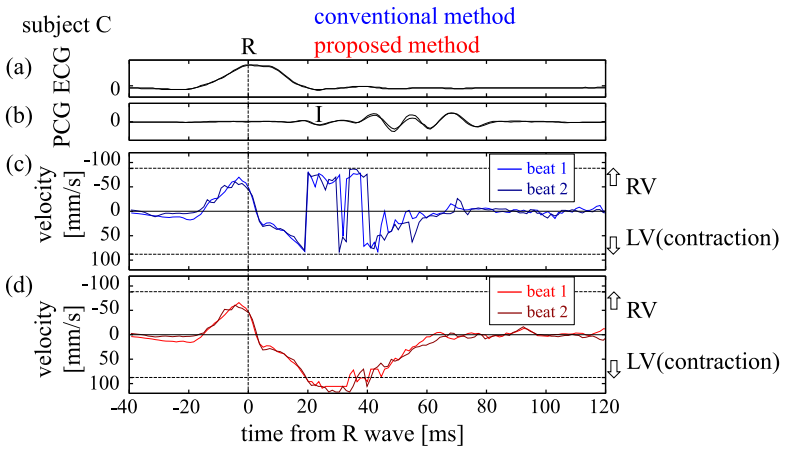

Fig. 7. Results of the estimated velocity waveform for subject C in two consecutive heartbeats. (a) Electrocardiogram (ECG) waveform. (b) Phonocardiogram (PCG) waveform. (c) Velocity waveform estimated using the conventional method that uses the phase difference at the center frequency of the transmitted signal. (d) Velocity waveform estimated using the proposed method that uses phase differences with multiple frequencies. LV = left ventricle; RV = right ventricle.

over frames around the time phase of the ECG R-wave were 7.3 (conventional) and 1.8 (proposed) in subject D, 7.7 (conventional) and 3.0 (proposed) in subject E, and 6.5 (conventional) and 2.8 (proposed) in subject F, respectively. In three subjects, the SD in the proposed method was smaller than that in the conventional method. Therefore, we concluded that the velocity estimation using the proposed method was more precise than that obtained by the conventional method. For subjects A, B and C, the SD was not calculated because the RF data were acquired in only two heartbeats.

In the velocity waveforms estimated using the proposed method, the positive velocity toward the LV was observed during −30 to 0 ms from the ECG R-wave, as illustrated in Figures 5d, 6d and 7d. In our previous studies, it was suggested that this velocity was related to the minute contraction response caused by electrical excitation (Kanai and Tanaka 2011; Matsuno et al. 2017; Hayashi et al. 2019). In our future work, we will validate the relationship between the velocity waveforms and the actual electrical excitation. The precise velocity estimation by the proposed method would contribute to revealing this relationship.

DISCUSSION

Improvement of velocity estimation using phase differences with multiple frequencies

The proposed method improved velocity estimation because it accounted for the effects of attenuation and interference, which are not considered in the conventional method.

In the conventional phased-tracking method that uses the phase at the center frequency f_c of the transmitted signal, the estimation accuracy is negatively affected by the frequency-dependent attenuation. In Figure 4d, the peak frequency f_p of the received signal is lower than the center frequency f_c of the transmitted signal. This is because higher-frequency components were more affected by the attenuation when propagating in the living tissue. Therefore, the SNR at the center frequency of the transmitted signal was lower, and the velocity estimation accuracy was lower in the conventional method, which used only the phase at the center frequency of the transmitted signal.

The effect of the interference with other backscattered waves should be discussed in the measurement of heart wall measurements. The main scatterers in the myocardium are collagen fibers. The myocardium has a layered structure, consisting of several myocardial fibers, and there are abundant collagen fibers between the layers. Because collagen fibers are smaller than the ultrasound spatial resolution, the signals received from the myocardium with numerous scattered waves interfere with each other, and the B-mode image exhibits a speckle pattern. The scattered waves can build up (constructive interference, or in-phase waves) or cancel out (destructive interference, or out-of-phase waves). Therefore, the specific frequency component of the cross-spectrum decreases depending on the spacing among the numerous scatterers in the myocardium. In Figures 4b and 4d, the frequency spectrum amplitude $|S_n(f)|$, $|S_{n+1}(f)|$ and the cross-spectrum amplitude $|C_n(f)|$ decreased at the center frequency of the transmitted signal. This occurred owing to the destructive interference at the analyzed position, especially at the center frequency of the transmitted signal. Thus, the phase difference calculated at the center frequency of the

transmitted signal would be affected by the background noise.

A notable disadvantage of the conventional method is not only to use the phase difference at the center frequency of the transmitted signal but also to use the phase difference for only a single frequency of the received signal. In the heart wall, rapid changes in the wall thickness associated with myocardial contraction change the spacing among the scatterers. Because the amplitude of the myocardial strain rate exceeds 4 (m/s)/m when measured in the left ventricular long-axis view (Yoshiara et al. 2007; Tanaka et al. 2014a, 2014b, 2017), an approximately 10-μm change in thickness in the spatial window occurs over 1 ms; thus, changes in the interference state between two consecutive frames occur even for high-frame-rate measurements. Even if the SNR is not low, a change in the interference between two consecutive frames induces a phase difference that is different from that caused by the actual heart wall motion. Because of the state of the interference changes owing to rapid changes in heart wall thickness, the conventional phased-tracking method (Kanai et al. 1996, 1997) and the phased-tracking method that was developed for addressing arterial wall thickness changes (Hasegawa et al. 2002; Hasegawa and Kanai 2006) would be difficult to apply to heart wall measurements.

In the proposed method, the phased-tracking method extended to multiple frequencies alleviated the negative effects of attenuation and interference on estimation accuracy. Because the velocity is estimated from the phases with multiple frequencies using the cross-spectrum amplitude $|C_n(f)|$ as a weighting function, the influence of the phase at the frequency where the SNR decreases owing to attenuation and interference is alleviated. Furthermore, the influence of the change in the interference state is alleviated when estimating the velocity based on the phase differences with multiple frequencies. If the phase difference caused by the change in the interference state is random at different frequencies, combining the phase differences for several frequencies is likely to be useful for suppressing the effect of the change in the interference state. As a result, smooth waveforms (without spike-like velocity changes) were obtained with high precision.

Figure 8 illustrates (a) the ECG waveform, (b) the PCG waveform, (c) the velocity waveform, (d) the RMSE of the phase gradient estimation and (e) the depth of the tracking point during a cardiac cycle for subject D. In the conventional method, the depth of the tracking point did not return to its original position after one cardiac cycle. Because the displacement is obtained by integrating the velocity waveform, an erroneous velocity estimation leads to an unrepairable error in tracking the analyzed point. The deviation from the original position after one cardiac cycle was improved by the proposed method compared with the conventional method in subject D, as illustrated in Figure 8e, and similar results were confirmed in other five subjects. Therefore, we concluded that the proposed method has the potential to estimate the velocity with higher accuracy than the conventional method. In our future work, the accuracy of velocity estimation using the proposed method will be evaluated by the simulation or the experiment using a phantom which has a local change in thickness.

Usefulness in measurements of myocardial contraction

We examined the usefulness of the proposed method for estimating the velocity for measuring the heart wall's

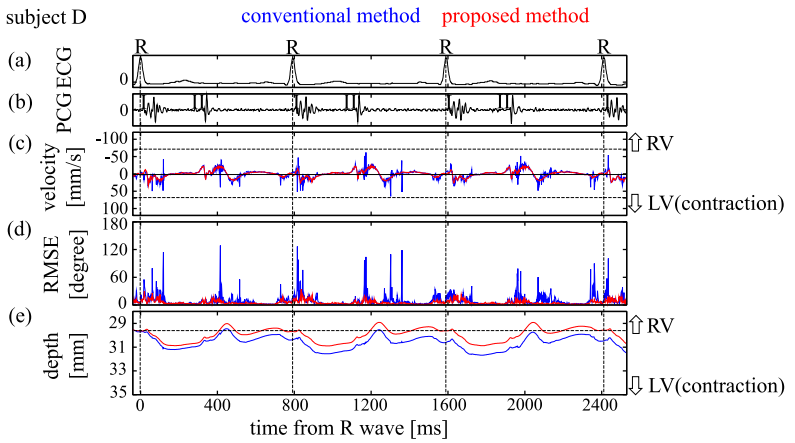

Fig. 8. Results of the estimated velocity waveform for subject D during a cardiac cycle. (a) Electrocardiogram (ECG) waveform. (b) Phonocardiogram (PCG) waveform. (c) Velocity waveform. (d) Minimal root mean square error (RMSE) of the phase gradient estimation. (e) Depth of the analyzed point, where *blue lines* represent the results obtained using the conventional method that uses the phase difference at the center frequency of the transmitted signal, while the *red lines* represent the results obtained using the proposed method that uses phase differences with multiple frequencies.

contraction response. The myocardial contraction response was measured by calculating the myocardial strain rate (Kanai et al. 1997; Sutherland et al. 2004; Yoshiara et al. 2007; Tanaka et al. 2014a, 2014b, 2017) and the minute contraction propagation speed from the velocity waveforms at multiple heart wall locations (Matsuno et al. 2017; Hayashi et al. 2019). However, because the velocity waveforms obtained using the conventional method are affected by attenuation and interference, as mentioned above, it was difficult to reliably estimate the myocardial strain rate and the minute contraction propagation velocity from the velocity estimated at a single measurement point. For this reason, when measuring the contraction response using the conventional method, the phase $\angle C_n(f_c)$ at the center frequency of the transmitted signal was spatially averaged around the analysis point in the depth direction, and the cross-correlation function was used for estimating the spatially averaged velocity (Kanai et al. 1996, 1997).

The usefulness of the proposed method in measuring the change in thickness of the heart wall was validated by measuring the transmural thickness of the heart wall using the conventional and proposed methods during a cardiac cycle in six healthy subjects. The change in wall thickness was calculated from the differences between the velocity waveforms at the LV side and the RV side of the IVS. Figure 9 illustrates results for subject D with (a) the ECG waveform, (b) the PCG waveform, (c) the velocity waveforms estimated using the conventional method with spatial averaging, (d) the velocity waveforms estimated using the proposed method and (e) the thicknesses of the heart wall for subject D. The results in Figure 9c, 9d illustrate the positive velocity waveforms toward the LV (contraction) during the ejection period, and then the negative velocity waveforms toward the RV during the filling period. Because the amplitude of the velocity at the LV side was larger than that at the RV side during the ejection and filling periods, the thickness increased during the ejection period and decreased during the filling period, as illustrated in Figure 9e. Around the time phase of the ECG R-wave, there was almost no change in the thickness.

The waveform of the thickness measured by the proposed method was similar to that measured using ultrasonic crystals in the previous studies (Sasayama et al. 1976; Hartley et al. 1983, 1991). The thickness measured using the proposed method (*red line*) returned to the original thickness after one cardiac cycle, but that measured using the conventional method (*black line*) did not. These results were confirmed in six subjects. In the six healthy subjects, the thickening fraction (Hartley et al. 1983) was evaluated. The thickening fractions using the proposed method were in the range 20%−38%. The values of thickening fraction agreed with those in previous studies using ultrasonic crystals: 30% in dogs (Sasayama et al. 1976), 23%−38% in piglets (Hartley et al. 1983) and 20% in dogs (Hartley et al. 1991), respectively. Therefore, it was suggested that the proposed method was useful in measuring the change in the thickness of the heart wall.

The averaging effect of the velocity is discussed in Figure 10. The *black line* in Figure 10b represents the velocity waveform obtained using the conventional method with spatial averaging. In the conventional method with spatial averaging (*black line* in Fig. 10b), the cross-spectra at the center frequency of the transmitted signal were averaged in the range of ±1.22 mm from the analysis point in

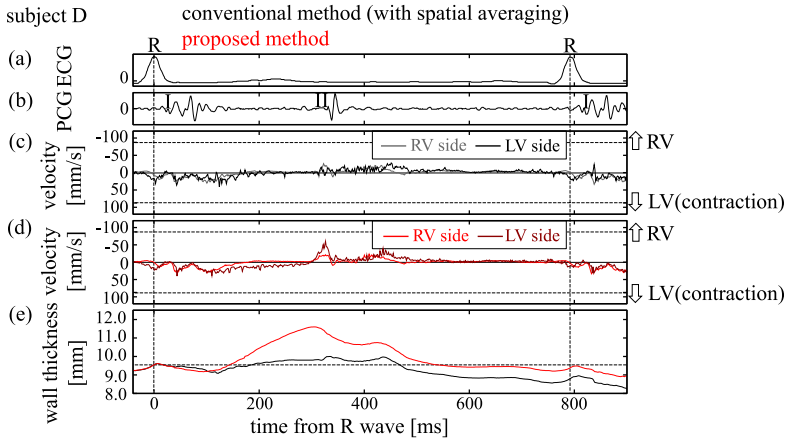

Fig. 9. Results of the estimated velocity waveform and the thickness of the heart wall for subject D during a cardiac cycle. (a) Electrocardiogram (ECG) waveform. (b) Phonocardiogram (PCG) waveform. (c) Velocity waveform estimated using the conventional method that uses the phase difference at a single center frequency of the transmitted signal with spatial averaging for cross-correlation function. (d) Velocity waveform estimated using the proposed method that uses phase differences with multiple frequencies. (e) Thickness of heart wall estimated using the distance from the depth of the analyzed point at the right ventricle (RV) side to that at the left ventricle (LV) side.

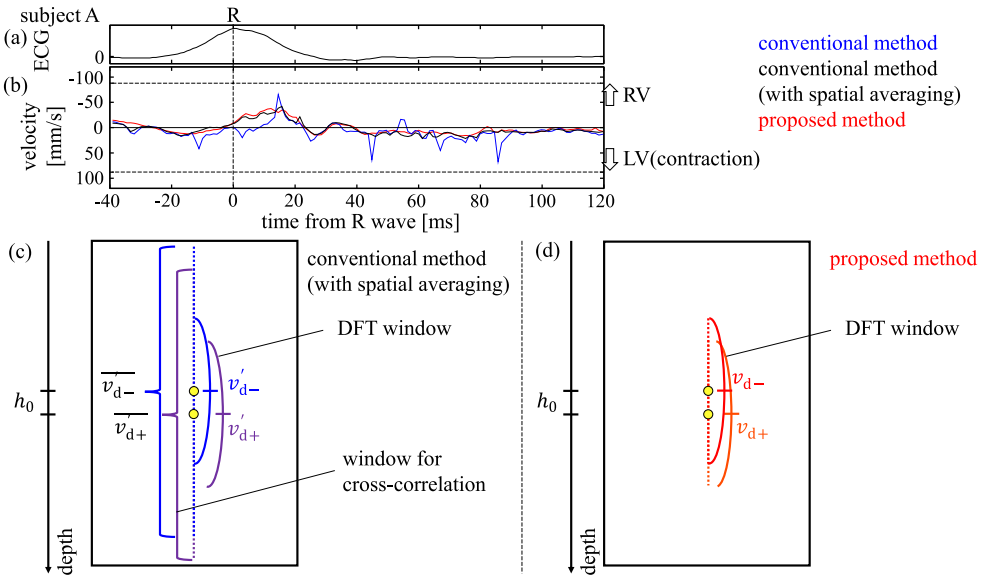

Fig. 10. (a) Electrocardiogram (ECG) waveform. (b) Velocity waveform. The *blue line* represents the results obtained using the conventional method that uses the phase difference at the center frequency of the transmitted signal. The *black line* represents the averaged results for velocities in the depth direction obtained using the conventional method that uses the phase difference at the center frequency of the transmitted signal. The *red line* represents the results obtained using the proposed method that uses phase differences with multiple frequencies. (c) Conceptual diagram of the calculation of the myocardial strain rate using the conventional method. (d) Conceptual diagram of the calculation of the myocardial strain rate using the proposed method. *Yellow circles* represents the analyzed points at which the velocity was estimated. DFT = discrete Fourier transform; LV = left ventricle; RV = right ventricle.

the depth direction. As illustrated in Figure 10b, spike-like velocity changes estimated using the conventional method were alleviated by spatial averaging.

There are differences between the velocity waveform estimated using the conventional method with spatial averaging and that estimated using the proposed method without spatial averaging. This is attributed to changes in the heart wall thickness that are associated with myocardial contractions. If the velocity is uniform, that is, if the thickness does not change, within the range of averaging, the accuracy of the velocity estimation at the analysis point is improved by averaging. However, because the heart wall thickness changes locally owing to contractions, the velocities in the averaging range in the depth direction differ depending on the depth, and the accuracy of the velocity estimation at the analysis point decreases with averaging. Because the proposed method can yield smooth velocity waveforms without averaging, the velocity can be estimated locally, for example, at a single point, compared with the conventional method. Thus, the proposed velocity estimation method with multiple frequencies is useful for measuring heart wall dynamics that involve thickness changes.

Finally, let us discuss how the proposed method improves the locality in measuring the heart wall dynamics by considering the myocardial strain rate measurement as an example. The myocardial strain rate of the nth frame, $SR(n)$, is calculated using the velocity $v_{d+}(n)$ at the deep analysis point, the velocity $v_{d-}(n)$ at the shallow analysis point and the distance h_0 between their two points (Yoshiara et al. 2007; Tanaka et al. 2014a, 2014b, 2017), as

$$SR\,(n) = \frac{v_{d+}(n) - v_{d-}(n)}{h_0}. \tag{7}$$

In previous studies, the distance h_0 between the two points was only 821 μm. Figure 10c, 10d illustrates the conceptual diagram of ranges of velocities used for calculating the myocardial strain rate in the conventional and proposed methods. Because the analyzed region in the conventional method was averaged in the depth direction, the velocity estimated at the analysis point included different velocities in the averaging window, as illustrated in Figure 10c. When the DFT window is ±1.22 mm for the velocity estimation, the overlaps between the two windows in the myocardial strain rate measurements are 83% and 66% for the conventional and proposed methods, respectively. The proposed method estimated the velocity at the analysis point in a more local manner. Therefore, the myocardial strain rate is calculated more locally in the proposed method, compared with the conventional method. In our future work, the local strain rate will be measured using the proposed method.

Clinical application

The proposed method is applicable to existing ultrasonic diagnostic apparatuses with only the software upgrade for use offline. For use in real time, a hardware board may be a need if the computational capacity is insufficient in the existing ultrasonic diagnostic apparatus. This velocity estimation procedure can be achieved by digital signal processing so it is not difficult to implement our proposed method in existing ultrasonic diagnostic apparatuses. In the clinical application, first, the region of interest (ROI) is set on the heart wall, and the velocities in the top and the bottom of the ROI are estimated using the proposed method. Then, the thickening (strain) or strain rate in the ROI is calculated from the velocities.

The velocity estimated using the proposed method has the parallel component to the ultrasound beam. In the previous study, it was confirmed that the strain and strain rate calculated from the velocities in the ultrasound beam direction have the potential to quantify myocardial ischemia and to evaluate the LV mass regression after treatments (Sutherland et al. 2004). It is possible to expand the proposed method to the 2-D motion estimator using the 2-D Fourier transform (Hasegawa 2016), if needed.

CONCLUSIONS

In the present study, we proposed a velocity estimation method that alleviates the effects of attenuation and interference, which negatively affect the velocity estimation in the conventional method that uses the phase difference at the center frequency of the transmitted signal. Using the proposed method, in which the velocity was estimated using the phase differences with multiple frequencies, we were able to obtain the velocity waveform in the direction of the ultrasound beam in the heart wall with high precision. Moreover, it was confirmed that the estimation precision of the conventional velocity estimation method using the phase difference at the center frequency of the transmitted signal decreased owing to the frequency-dependent attenuation and interference of scattered waves.

The proposed method can estimate the local velocity waveform of the myocardium without averaging in the depth direction, while the conventional method requires averaging. This locality of velocity estimation is essential for measuring the dynamics of the heart wall that exhibits thickness changes because the velocity depends on the analyzed point.

Acknowledgments—This work was supported in part by Japan Society for the Promotion of Science (JSPS) KAKENHI 19 K22943.

Conflict of interest disclosure—The authors declare that they have no competing interests.

REFERENCES

Durrer D, van Dam RT, Freud GE, Janse MJ, Meijler FL, Arzbaecher RC. Total excitation of the isolated human heart. Circulation 1970;41:899–912.

Faris OP, Evans FJ, Ennis DB, Helm PA, Taylor JL, Chesnick AS, Guttman MA, Ozturk C, McVeigh ER. Novel technique for cardiac electromechanical mapping with magnetic resonance imaging tagging and an epicardial electrode sock. Ann Biol Eng 2003;31:430–440.

Foreman KJ, Marquez N, Dolgert A, Fukutaki K, Fullman N, McGaughey M, Pletcher MA, Smith AE, Tang K, Yuan CW, Brown JC, Friedman J, He J, Heuton KR, Holmberg M, Patel DJ, Reidy P, Carter A, Cercy K, Chapin A, Douwes-Schultz D, Frank T, Goettsch F, Liu PY, Nandakumar V, Reitsma MB, Reuter V, Sadat N, Sorensen RJD, Srinivasan V, Updike RL, York H, Lopez AD, Lozano R, Lim SS, Mokdad AH, Vollset SE, Murray CJL. Forecasting life expectancy, years of life lost, and all-cause and cause-specific mortality for 250 causes of death: Reference and alternative scenarios for 2016–40 for 195 countries and territories. Lancet 2018;392:2052–2090.

Grondin J, Wan E, Gambhir A, Garan H, Konofagou EE. Intracardiac myocardial elastography in canines and humans in vivo. IEEE Trans Ultrason Ferroelectr Freq Control 2015;62:337–349.

Grondin J, Wang D, Grubb CS, Trayanova N, Konofagou EE. 4D cardiac electromechanical activation imaging. Comput Biol Med 2019;113:1–14.

Guth B, Savage R, White F, Hagan A, Samtoy L, Bloor C. Detection of ischemic wall dysfunction: Comparison between M-mode echocardiography and sonomicrometry. Am Heart J 1984;107:449–457.

Hartley CJ, Latson LA, Michael LH, Seidel CL, Lewis RM, Entman ML. Doppler measurement of myocardial thickening with a single epicardial transducer. Am J Physiol 1983;245:HlO66–H1072.

Hartley CJ, Litowitz H, Rabinovitz RS, Zhu W-X, Chelly JE, Michael LH, Bolli R. An ultrasonic method for measuring tissue displacement: Technical details and validation for measuring myocardial thickening. IEEE Trans Biomed Eng 1991;38:735–747.

Hasegawa H. Phase-sensitive 2D motion estimators using frequency spectra of ultrasonic echoes. Appl Sci 2016;6:195.

Hasegawa H, Kanai H. Improving accuracy in estimation of artery-wall displacement by referring to center frequency of RF echo. IEEE Trans Ultrason Ferroelectr Freq Control 2006;53:52–63.

Hasegawa H, Kanai H. Reduction of influence of variation in center frequencies of RF echoes on estimation of artery-wall strain. IEEE Trans Ultrason Ferroelectr Freq Control 2008a;55:1921–1934.

Hasegawa H, Kanai H. Simultaneous imaging of artery-wall strain and blood flow by high frame rate acquisition of RF signals. IEEE Trans Ultrason Ferroelectr Freq Control 2008b;55:2626–2639.

Hasegawa H, Kanai H, Koiwa Y. Modified phased tracking method for measurement of change in thickness of arterial wall. Jpn J Appl Phys 2002;41:3563–3571.

Hayashi A, Mori S, Arakawa M, Kanai H. Local Two-dimensional distribution of propagation speed of myocardial contraction for ultrasonic visualization of contraction propagation path. Jpn J Appl Phys 2019;58:SGGE05.

Heyndrickx GR, Millard RW, McRitchie RJ, Maroko PR, Vatner SF. Regional myocardial functional and electrophysiological alterations after brief coronary artery occlusion in conscious dogs. J Clin Invest 1975;56:978–985.

Homans DC, Asinger R, Elsperger KJ, Erlien D, Sublett E, Mikell F, Bache RJ. Regional function and perfusion at the lateral border of ischemic myocardium. Circulation 1985;71:1038–1047.

Jamal F, Kukulski T, Sutherland GR, Weidemann F, D'hooge J, Bijnens B, Derumeaux G. Can changes in systolic longitudinal deformation quantify regional myocardial function after an acute infarction? An ultrasonic strain rate and strain study. J Am Soc Echocardiogr 2002;15:723–730.

Kanai H, Tanaka M. Minute mechanical-excitation wave-front propagation in human myocardial tissue. Jpn J Appl Phys 2011;50 07HA01.

Kanai H, Sato M, Koiwa Y, Chubachi N. Transcutaneous measurement and spectrum analysis of heart wall vibrations. IEEE Trans Ultrason Ferroelectr Freq Control 1996;43:791–810.

Kanai H, Hasegawa H, Chubachi N, Koiwa Y, Tanaka M. Noninvasive evaluation of local myocardial thickening and its color-coded imaging. IEEE Trans Ultrason Ferroelectr Freq Control 1997;44:752–768.

Kanai H, Hasegawa H, Imamura K. Spatial distribution measurement of heart wall vibrations generated by remote perturbation of inner pressure. Jpn J Appl Phys 2006;45:4718–4721.

Konofagou EE, Provost J. Electromechanical wave imaging for noninvasive mapping of the 3D electrical activation sequence in canines and humans in vivo. J Biomech 2012;45:856–864.

Marwick TH. Measurement of strain and strain rate by echocardiography: Ready for prime time?. J Am Coll Cardiol 2006;47:1313–1327.

Mason SJ, Weiss JL, Weisfeldt ML, Garrison JB, Fortuin NJ. Exercise echocardiography: Detection of wall motion abnormalities during ischemia. Circulation 1979;59:50–59.

Matsuno Y, Taki H, Yamamoto H, Hirano M, Morosawa S, Shimokawa H, Kanai H. Ultrasound imaging of propagation of myocardial contraction for non-invasive identification of myocardial ischemia. Jpn J Appl Phys 2017;56 07JF05.

McVeigh E, Faris O, Ennis D, Helm P, Evans F. Electromechanical mapping with MRI tagging and epicardial sock electrodes. J Electro Cardiol 2002;35:61–64.

Pernot M, Fujikura K, Fung-Kee-Fung SD, Konofagou EE. ECG-gated, mechanical and electromechanical wave imaging of cardiovascular tissues in vivo. Ultrasound Med Biol 2007;33:1075–1085.

Picano E, Lattanzi F, Orlandini A, Marini C, L'Abbate A. Stress echocardiography and the human factor: The importance of being expert. J Am Coll Cardiol 1991;17:666–669.

Pislaru C, Bruce CJ, Anagnostopoulos PC, Allen JL, Seward JB, Pellikka PA, Ritman EL, Greenleaf JF. Ultrasound strain imaging of altered myocardial stiffness stunned versus infarcted reperfused myocardium. Circulation 2004;109:2905–2910.

Ramanathan C, Ghanem RN, Jia P, Ryu K, Rudy Y. Noninvasive electrocardiographic imaging for cardiac electrophysiology and arrhythmia. Nat Med 2004;10:422–428.

Sabbah HN, Marzilli M, Stein PD. The relative role of subendocardium and subepicardium in left ventricular mechanics. Am J Physiol 1981;240:H920–H926.

Salles S, Chee AJY, Garcia D, Yu ACH, Vray D, Liebgott H. 2-D arterial wall motion imaging using ultrafast ultrasound and transverse oscillations. IEEE Trans Ultrason Ferroelectr Freq Control 2015;62:1047–1058.

Sasayama S, Franklin D, Ross J, Jr, Kemper WS, McKown D. Dynamic changes in left ventricular wall thickness and their use in analyzing cardiac function in the conscious dog. Am J Cardiol 1976;38:870–879.

Shapiro E, Marier DL, St John Sutton MG, Gibson DG. Regional non-uniformity of wall dynamics in normal ventricle. Br Heart J 1981;45:264–270.

Sutherland GR, Salvo GD, Claus P, D'hooge J, Bijnens B. Strain and strain rate imaging: A new clinical approach to quantifying regional myocardial function. J Am Soc Echocardiogr 2004;17:788–802.

Tanaka M, Sakamoto T, Sugawara S, Katahira Y, Tabuchi H, Nakajima H, Kurokawa T, Kanai H, Hasegawa H, Ohtsuki S. A new concept of the contraction-extension property of the left ventricular myocardium. J Cardiol 2014a;63:313–319.

Tanaka M, Sakamoto T, Sugawara S, Katahira Y, Tabuchi H, Nakajima H, Kurokawa T, Kanai H, Hasegawa H, Ohtsuki S. Non-uniform distribution of the contraction/extension (C-E) in the left ventricular myocardium related to the myocardial function. J Cardiol 2014b;64:401–408.

Tanaka M, Sakamoto T, Sugawara S, Katahira Y, Hasegawa K, Nakajima H, Kurokawa T, Kanai H, Hasegawa H. Deformability of the pulsating left ventricular wall: A new aspect elucidated by high resolution ultrasonic methods. J Cardiol 2017;69:462–470.

Tanaka M, Sakamoto T, Saijo Y, Katahira Y, Sugawara S, Nakajima H, Kurokawa T, Kanai H. Role of intra-ventricular vortex in left ventricular ejection elucidated by echo-dynamography. J Med Ultrason 2019;46:413–423.

Theroux P, Franklin D, Ross J, Jr, Kemper WS. Regional myocardial function during acute coronary artery occlusion and its modification by pharmacologic agents in the dog. Circ Res 1974;35:896–908.

Yoshiara H, Hasegawa H, Kanai H. Ultrasonic imaging of propagation of contraction and relaxation in the heart walls at high temporal resolution. Jpn J Appl Phys 2007;46:4889–4896.